Geophysical Research Letters

RESEARCH LETTER
10.1029/2022GL099530

Cryogeomorphic Characterization of Shadowed Regions in the Artemis Exploration Zone

V. T. Bickel[1], B. Moseley[2], E. Hauber[3], M. Shirley[4], J.-P. Williams[5], and D. A. Kring[6]

[1]ETH Zurich, Zurich, Switzerland, [2]University of Oxford, Oxford, UK, [3]German Aerospace Center, Berlin, Germany, [4]NASA Ames Research Center, Mountain View, CA, USA, [5]University of California Los Angeles, Los Angeles, CA, USA, [6]Lunar and Planetary Institute, USRA, Houston, TX, USA

Key Points:

- We produce the first high-signal-to-noise ratio and -resolution orbital images over 44 shadowed regions within the Artemis exploration zone using an AI tool
- We characterize the meter-scale (cryo) geomorphology of those regions including surface texture, fresh craters, boulders, and relative age
- Our data are freely available and can be used to support future science and mission planning efforts in the area

Supporting Information:

Supporting Information may be found in the online version of this article.

Correspondence to:

V. T. Bickel,
valentin.bickel@erdw.ethz.ch

Citation:

Bickel, V. T., Moseley, B., Hauber, E., Shirley, M., Williams, J.-P., & Kring, D. A. (2022). Cryogeomorphic characterization of shadowed regions in the Artemis exploration zone. *Geophysical Research Letters*, *49*, e2022GL099530. https://doi.org/10.1029/2022GL099530

Received 15 MAY 2022
Accepted 21 JUL 2022

Author Contributions:

Conceptualization: V. T. Bickel
Data curation: V. T. Bickel, B. Moseley, J.-P. Williams
Formal analysis: V. T. Bickel, E. Hauber, M. Shirley, J.-P. Williams, D. A. Kring
Funding acquisition: V. T. Bickel, B. Moseley
Investigation: V. T. Bickel, E. Hauber, M. Shirley, J.-P. Williams, D. A. Kring
Methodology: V. T. Bickel, B. Moseley
Resources: V. T. Bickel, B. Moseley
Software: V. T. Bickel, B. Moseley
Validation: V. T. Bickel

Abstract The Artemis program will send crew to explore the south polar region of the Moon, preceded by and integrated with robotic missions. One of the main scientific goals of future exploration is the characterization of polar volatiles, which are concentrated in and near regions of permanent shadow. The meter-scale cryogeomorphology of shadowed regions remains unknown, posing a potential risk to missions that plan to traverse or land in them. Here, we deploy a physics-based, deep learning-driven post-processing tool to produce high-signal and high-resolution Lunar Reconnaissance Orbiter Narrow Angle Camera images of 44 shadowed regions larger than ~40 m across in the Artemis exploration zone around potential landing sites 001 and 004. We use these images to map previously unknown, shadowed meter-scale (cryo)geomorphic features, assign relative shadowed region ages, and recommend promising sites for future exploration. We freely release our data and a detailed catalog of all shadowed regions studied.

Plain Language Summary In the next couple of years a large number of robotic missions and payloads will be delivered to the Moon, ultimately culminating in crewed missions. Those missions aim at characterizing lunar polar volatiles, which are concentrated in regions of permanent shadow. However, the small-scale surface properties of shadowed regions remain largely unknown. The lack of knowledge poses a potential risk to future ground-based missions that seek to enter shadowed regions. Here, we use a machine learning-driven algorithm to remove noise from previously largely unusable satellite images of shadowed regions. We use those de-noised images to study the surface properties of 44 small, shadowed regions in the Artemis exploration zone close to the lunar south pole for the first time, identifying potential hazards, and recommending sites for future exploration missions. We freely release our images along with a detailed catalog of the shadowed regions studied.

1. Introduction

Future missions and payloads delivered to the Moon, such as VIPER, IM-2 (S. P. HOPPER and PRIME-1), PROSPECT, LUPEX, Chandrayaan-3, LunaH-Map, IceCube, and Trailblazer (e.g., Colaprete et al., 2021; Ehlmann et al., 2022; Martin et al., 2022), seek to characterize lunar (south) polar volatiles (NASA, 2020a). Volatiles may be concentrated in cold traps within permanently shadowed regions (PSRs) that may not have received sunlight in millions to potentially billions of years (Arnold, 1979; Feldman et al., 2011; Watson et al., 1961). S. P. Hopper, a hopper robot developed by Intuitive Machines, is planned to hop and land in a small PSR as early as late 2022 or early 2023 (Martin et al., 2022). NASA's Volatile Investigating Polar Exploration Rover (VIPER) is bound to traverse a series of PSRs in late 2023 (Colaprete et al., 2021). Most notably, the Artemis program will land humans on the south polar surface by ~2025 somewhere in the so-called Artemis exploration zone, that is, the region poleward of ~84°S (NASA, 2020a, 2020b). Currently, most science and mission planning efforts for a crewed and a number of robotic missions focus on a ridge adjacent to Shackleton crater (e.g., Bickel & Kring, 2020; Gawronska et al., 2020; Scoville, 2022; Speyerer & Robinson, 2013; Spudis et al., 2008). Mazarico et al. (2011) identified two topographically elevated points (sites 001 and 004) in that area which would provide optimal illumination and Direct-To-Earth communications. The area around sites 001 and 004 hosts a large number of PSRs with diameters ranging from a few meters (micro-PSRs, see, e.g., Hayne et al., 2020) to ~1.3 km (small PSRs) which could be potential targets for future missions.

Due to the lack of primary illumination, PSRs are difficult to image using high-resolution optical sensors (Cisneros et al., 2017; Haruyama et al., 2008; Martin et al., 2021). The lack of high-resolution images opens a

Visualization: V. T. Bickel, J.-P. Williams
Writing – original draft: V. T. Bickel, B. Moseley, E. Hauber, M. Shirley, J.-P. Williams, D. A. Kring
Writing – review & editing: V. T. Bickel, B. Moseley, E. Hauber, M. Shirley, J.-P. Williams, D. A. Kring

strategic knowledge gap: currently, the meter-scale (<∼5 m) cryogeomorphology of PSRs in the Artemis exploration zone and beyond remains largely unknown. Detailed knowledge about the cryogeomorphic characteristics of PSRs would allow for: (a) the selection of target PSRs, putting constraints on potential landing sites. (b) The identification of scientific targets—including small doubly shadowed regions, that is, primary and secondary illumination shielded, particularly cold regions—and potential hazards within target PSRs. (c) The planning of effective and safe traverses through target PSRs, including the PSR terminator, that is, the sunlight-shadow transition zone. (d) The overall reduction of the associated risk of operating in permanent shadow. (e) The contextualization of scientific measurements made by future ground and orbital missions.

Here, we address this strategic knowledge gap by deploying a recently developed, deep learning-based Lunar Reconnaissance Orbiter (LRO) Narrow Angle Camera (NAC) post-processing tool (called Hyper-effective nOise Removal Unet Software [HORUS]) to produce high-signal-to-noise ratio (SNR) and high-resolution images of selected shadowed regions in the Artemis exploration zone. We focus on 44 PSRs with diameters larger than ∼40 m in an area between Shackleton crater's rim, Spudis crater, and Henson crater, encompassing the Shackleton-Henson connecting ridge, around potential Artemis (001 & 004) and other landing sites (e.g., IM-2's S. P. Hopper and PRIME-1, see Figure 1) (NASA, 2020b). We only consider PSRs that are covered by at least 2 by 2 pixels in Mazarico et al. (2011)'s 60 m/pixel lunar orbiter laser altimeter (LOLA)-derived illumination product with two exemptions: a small PSR (X01a, ∼90 m across) in a crater that might be targeted by S. P. Hopper (Martin et al., 2022) and a very small PSR close to site 001 (X01b, ∼40 m across). We use the produced HORUS images to search for and map (cryo)geomorphic features such as surface ice/frost, boulders, craters, lobate features, and textured ground. We combine the mapping results with existing thermophysical and geological data, such as a new 1:8000 geomorphic map of the south pole (Bernhardt et al., 2022). The results are used to assign relative PSR ages and—ultimately—recommend potentially promising target PSRs for future missions. Our findings, PSR catalog, and HORUS data products are freely available (https://doi.org/10.56272/GQKZ6227) and will have direct implications on all future missions seeking to explore PSRs in the Artemis exploration zone and beyond.

2. Data and Methods

2.1. HORUS

HORUS is a deep learning-driven post-processing tool that ingests optical, short-exposure LRO NAC EDR regular and summed-mode images of shadowed regions, removes a variety of noise sources from them (significantly increasing their SNR), and outputs science-ready images (Bickel et al., 2021; Moseley et al., 2021) (Figure 2). Given a sufficient level of secondary illumination (between 10 and 15 pixel counts—data numbers or DN—or more), HORUS is able to resolve umbral features as small as ∼3 m across, while not adding any false features (false positives) (Bickel et al., 2021; Moseley et al., 2021). Illumination sources are secondary illumination from the Sun (backscattered by topography) and Earthshine. HORUS images feature spatial resolutions a factor 5–10 better than existing, long-exposure (LRO and Kaguya/Selene) images of PSRs (Cisneros et al., 2017; Haruyama et al., 2008; Martin et al., 2021). HORUS consists of two physics-based deep neural networks applied sequentially: (a) DestripeNet, which removes the dark noise in the images and (b) PhotonNet, which reduces all other noise sources (e.g., shot noise, read noise).

HORUS taps into an image archive of up to 200,000 images taken over the lunar poles over ∼13 years and can be used to address a variety of objectives, including mapping of PSR surface features, investigation of the origin of anomalous radar signatures in polar craters, detection of temporal changes in PSRs, provision of hazard and trafficability information, and characterization of landforms that may be indicative of permafrost-like processes, at least in small and relatively well secondary-lit PSRs. HORUS could complement observations made by future instruments such as ShadowCam, which has similar objectives (ShadowCam, 2022).

2.2. Image Validation

Due to a lack of ground truth data it is important to validate HORUS images, and Bickel et al. (2021) proposed multiple strategies for doing so. For this study, we verified features within each PSR by ensuring they were visible in at least two HORUS images (Figure S1 in Supporting Information S1). Individual features are not always visible as this depends on the direction and amount of secondary illumination. Features that were only observed in a single HORUS frame were classified as "potential/maybe." It is important to note that HORUS is not always

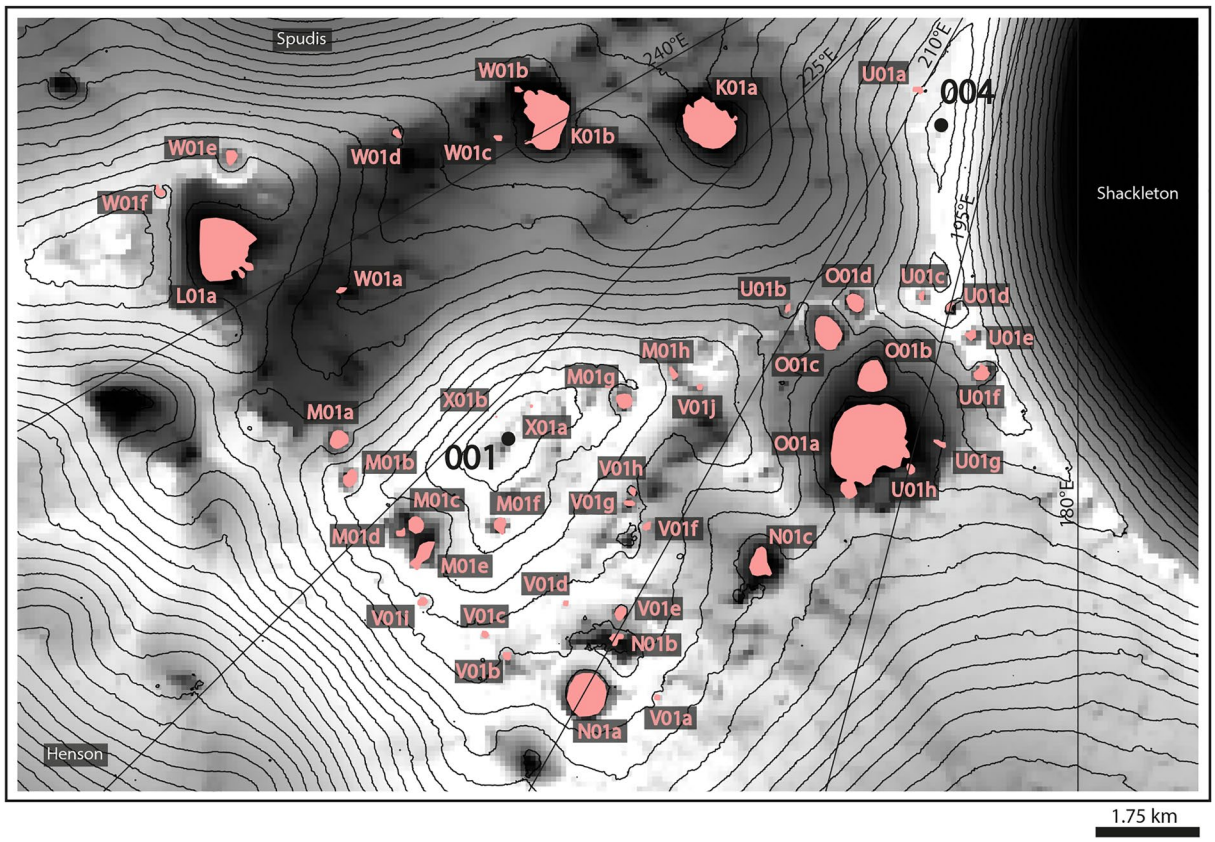

Figure 1. Overview map of the 44 studied permanently shadowed regions (PSRs) (>~100 m across, i.e., >2 by 2 pixels in the 60 m/pixel Sun visibility product of Mazarico et al. (2011), with exemption of sites X01a and X01b which are only ~90 and ~40 m across, respectively) in the studied section of the Artemis exploration zone (around sites 001 and 004, black dots; PSRs indicated in red, PSR IDs indicated in red). Five meridians indicated (180°E, 195°E, 210°E, 225°E, and 240°E). Lunar Reconnaissance Orbiter WAC percentage-based illumination map (black = no illumination, white = quasi-permanent illumination) in the background, black contour lines represent elevation changes of 100 m.

able to resolve very small features (<~9 m, false negatives), especially in poorly secondary-lit PSRs (as studied by Moseley et al. (2021)); in other words, if HORUS is not able to resolve features in a given area that does not necessarily mean there are no features at all (HORUS just does not resolve them).

2.3. Mapping and Analysis

Our mapping campaign searched for impact craters, boulders, lobate features, and textured surfaces, as well as any other, potentially interesting and/or anomalous feature, including ice exposures, surface frost, and mass wasting-related landforms. We further used existing thermophysical and geological/geomorphical data to assign relative PSR ages. The used datasets are topography, slope angle (Barker et al., 2021), surface roughness at 40 and 240 m (Smith & the LOLA Team, 2022), and the abundance of sunlit boulders, rocky craters, and outcrops around the PSRs, in combination with HORUS-derived umbral crater and boulder abundance (additional details shown in Figure S2 in Supporting Information S1).

We note that older PSRs are more likely to contain volatiles that were delivered by processes other than solar wind implantation, such as volcanic outgassing and cometary impacts (Needham & Kring, 2017). Older PSRs might also feature larger volumes of volatiles, because they had more time to accumulate (Cannon et al., 2020; Deutsch et al., 2020). At the same time, younger PSRs feature larger concentrations of boulders and outcrops which are attractive for sampling activities as well, or might have excavated volatiles from deeper layers that survive in ejecta. We point out that "older" PSRs located in impact craters—per our definition above—as well as craters within those PSRs are still geologically young due to their small size, <~100 Ma (Arvidson et al., 1975; Bogard & Hirsch, 1978; Drozd et al., 1974). Thus, these PSRs are significantly younger than the 1.8 ± 0.2–4.18 ± 0.02 Ga

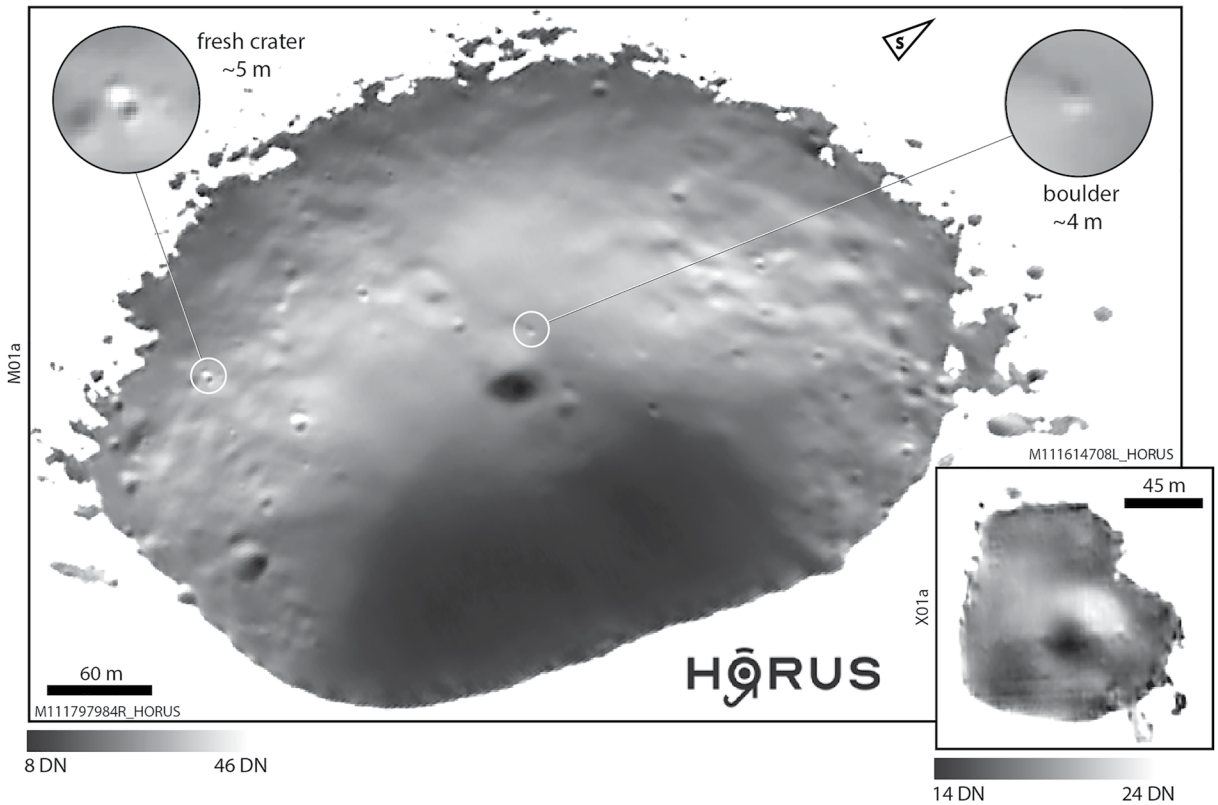

Figure 2. Hyper-effective nOise Removal Unet Software (HORUS) images of permanently shadowed regions (PSRs) M01a and X01a close to site 001. HORUS resolves boulders and craters as small as ~4–~5 m in those well secondary-lit PSRs, although parts of both PSRs remain shadowed/without signal. Some of the resolved craters in M01a appear to be fresher than other surrounding craters. HORUS resolves a large crater in X01a; X01a is a potential study site for IM-2's S. P. Hopper (Martin et al., 2022). The sunlight is incident from the ~E (M01a)/~S (X01a); the secondary illumination (visible in the HORUS images) is incident from the ~W (M01a)/~N (X01a). The white region around the PSR represents the oversaturated, sunlit surface. Raw Narrow Angle Camera image credits to NASA/LROC/GSFC/ASU.

old PSR-bearing craters with diameters of 20–108 km examined by Deutsch et al. (2020) and possibly younger than an additional set of <15 km diameter craters examined in that study with undetermined ages. We note that craters that formed within terrain of variable volatile content and temperature might differ in shape and morphology, potentially affecting our assessment of relative age.

Our exploration recommendations are based on a large number of HORUS-derived and thermophysical parameters, specifically: (a) surface ice detection/prediction, (b) temperature regime, (c) estimated PSR relative age, (d) relevant (cryo)geomorphic and/or geologic targets (boulders, fresh craters, geomorphic contacts), (e) trafficability (slope, roughness, estimated bearing capacity, hazards), (f) geographic location (overall accessibility, distance to 001/004), and (g) communications (Earth visibility). We do not rank those criteria, but present a variety of promising PSRs that excel in one or several of those criteria, or are remarkable for other reasons. All observations and findings are compiled in the Artemis exploration zone PSR catalog in the supplementary information (pages S12–S278).

3. Cryogeomorphology of the Artemis Exploration Zone Shadowed Regions

3.1. Crater, Boulder, and Lobate Feature Populations

We observed and mapped craters in 36 of the 44 studied PSRs (~82%). Most of the PSRs without craters are very small (<~0.02 km^2), making them less likely to accumulate craters. The majority of PSRs are located within impact craters themselves, but not all of them. The mapped umbral craters have diameters between ~5 and ~384 m. In the majority of PSRs the crater size frequency distribution (CSFD, available in the supplementary information) bends/rolls over at crater diameters of ~9–~11 m, similar to the observations made by Bickel

et al. (2021) in other south polar PSRs. This likely is an artifact of the resolution and denoising performance of HORUS, not caused by a physical process.

As an alternative to optical HORUS images Kereszturi et al. (2022) suggest mapping craters in LOLA-derived topography products, such as hillshades. They find that LOLA-based crater mapping in shadowed regions satisfactorily identifies craters with diameters between ∼100 and ∼200 m (only above ∼80°N and S, as the recognizable minimum crater size increases with decreasing latitude). This means that ∼96% of the craters identified in HORUS images of the studied Artemis exploration zone PSRs would have been missed with a LOLA-based approach, highlighting the importance of high-resolution and high-SNR optical images to recognize craters in permanent shadow.

Twenty-five PSRs feature small craters that might be geologically fresher—or younger—than the majority of craters as observed across the 44 PSRs. These potentially fresher craters are characterized by elevated rims and high overall reflectance (Figure S3 in Supporting Information S1), which might be caused by steep slopes and boulders <∼3 m (not directly resolved by HORUS). Some of those potentially fresher impact craters appear to be surrounded by higher-albedo ejecta blankets (Figure S4 in Supporting Information S1). It is unclear whether those impacts excavated icy material from the subsurface. We observed a number of sunlit rocky craters across the Shackleton-Henson connecting ridge; however, we did not recognize any (certain) umbral rocky craters, although PSR U01a might be a rocky crater itself.

Ten PSRs host visible boulders (∼23%), but this number could be significantly higher (41%), as a large number of potential boulders could only be mapped with a low level of confidence (e.g., were only visible in one HORUS image). We do not observe any signs of boulder displacement (e.g., boulder tracks), as identified in the sunlit south polar region around sites 001 and 004 (Bickel & Kring, 2020), so the geologic sources of the boulders are uncertain. The mapped umbral boulders feature diameters of ∼3–∼15 m. We note that we were not able to distinguish boulders and rocky outcrops—both features look very similar in secondary illumination conditions, that is, some of the mapped boulders might be rocky outcrops in reality, requiring further analysis.

We identified three PSRs that feature distinct lobate features. The geologic origin of two of those features (O01b, N01a, ∼175–∼450 m long) remains unclear, although the features appear to follow the local contour lines, that is, might be caused by/related to (slow) mass wasting (e.g., creep processes). We note that the PSRs and surrounding TSRs (transiently shadowed regions) in the studied section of the Artemis exploration zone appear to host fewer lobate features than were identified in other south polar regions (Bickel et al., 2021)—an initial observation that requires further confirmation. The lobate feature in PSR M01e appears to be the surface expression of a potential lobate scarp recently identified by Bernhardt et al. (2022) in the sunlit area around PSR M01e.

We identify distinctively textured ground in 11 PSRs/TSRs (25%). Here, textured ground is a rough (m-scale), undulating, unstructured surface (Figures S5–S7 in Supporting Information S1) that appears to predominantly occur on slopes around PSRs (within TSRs). Locally, we observe distinct and sharp umbral contacts between very smooth and highly textured surfaces (e.g., PSR W01e, Figures S5–S7 in Supporting Information S1). It remains unclear whether volatiles and temperature variations are involved in the formation of lobate features and textured ground and how both are connected to the apparent age of TSRs/PSRs (see, e.g., Bernhardt et al., 2022; Bickel et al., 2021).

The majority of the studied PSRs is located in/contains four different geomorphic units (Bernhardt et al., 2022): the crater floor ("cf"), cratered highlands ("chs"), moderately slope-textured surface ("mss"), and intensely slope-textured surface units ("iss"), but there is no distinct trend among those (Figure S8 in Supporting Information S1).

3.2. Presence of Ice and Surface Frost

Haruyama et al. (2008, 2013) examined the large PSR on the floor of Shackleton for high-albedo ice exposures using long-exposure 10 m/pixel SELENE Terrain Camera images. They did not find any exposed ice deposits, concluding that they either did not exist or that any water ice is disseminated in regolith in concentrations of only a few percent. Similar observations were made in LROC long-exposure data (Cisneros et al., 2017; Martin et al., 2021; Moon et al., 2020). We conducted a similar analysis for the PSRs in our study area, but were unable to locate any exposed surface ice or frost in the 44 studied PSRs, including PSRs that presumably feature ice

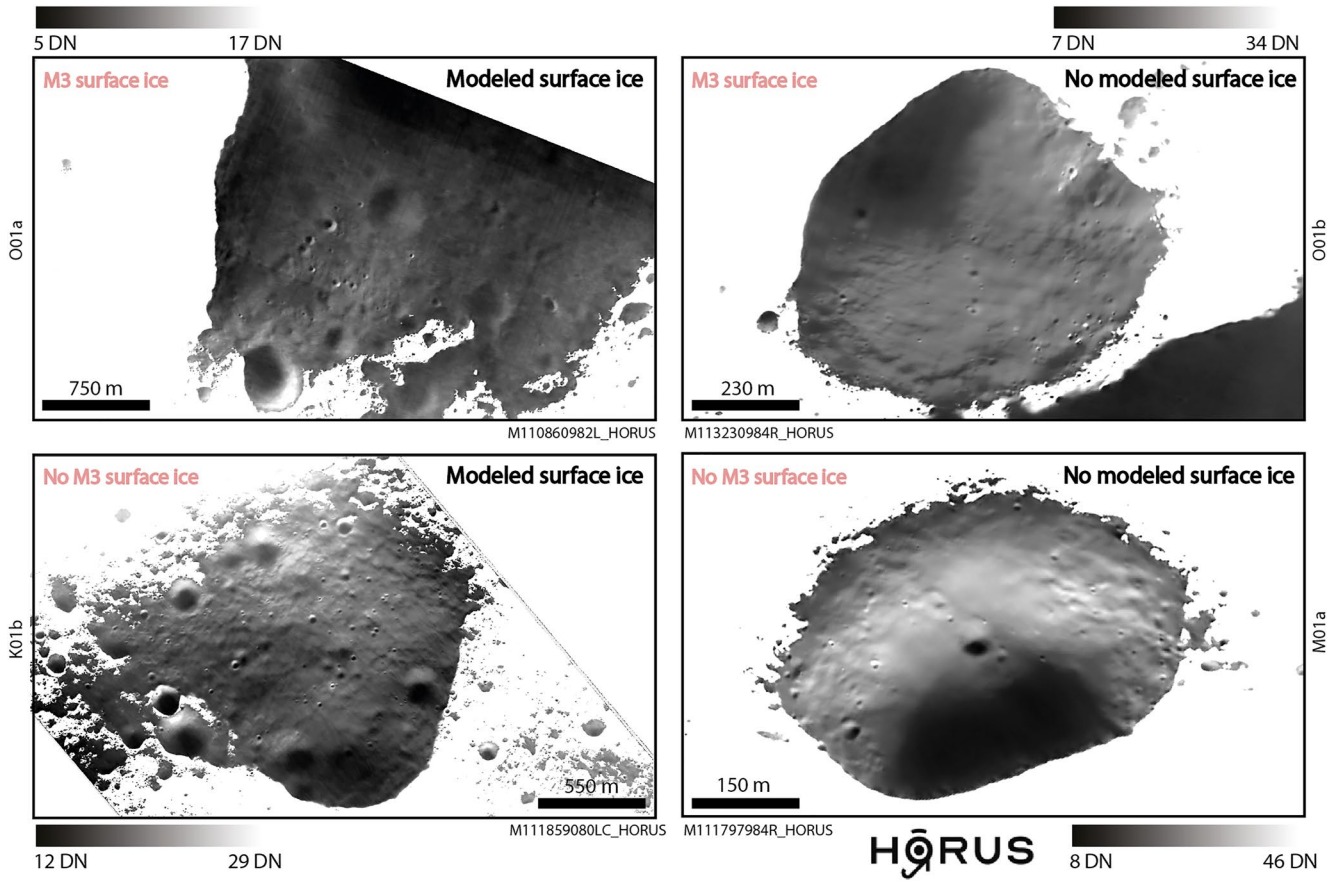

Figure 3. Comparison of the visible, meter-scale (cryo)geomorphology of presumably surface frost/ice-bearing permanently shadowed regions (M^3-observed and/or modeled; Li et al., 2018; Siegler et al., 2016) with a comparable (intermediate) relative age and size using Hyper-effective nOise Removal Unet Software (HORUS). Raw image credits to NASA/LROC/GSFC/ASU.

on their surfaces as observed by M^3 (Li et al., 2018) and modeled based on Diviner (Paige et al., 2010; Siegler et al., 2016). Further, we did not identify any clear difference in surface reflectance, albedo, crater abundance, or crater shape in PSRs with and without either M^3 surface ice detections and modeled surface/shallow sub-surface ice (Figure 3). Our observations provide further observational evidence that any umbral ice and volatiles that exist in the Artemis exploration zone may be intermixed with the regolith—or are buried at depth. Following Haruyama et al. (2008, 2013), an upper limit of a few percent ice in regolith is implied.

3.3. Relative PSR Ages

We identified 1 younger PSR (U01a, ~2%), 5 younger to intermediately old PSRs (M01b, M01g, V01a, V01b, ~11%), 11 intermediately old to older PSRs (~25%), and 4 older PSRs (M01h, N01c, U01g, V01j, ~9%). The remaining PSRs feature an intermediately old age; we point out that the majority of large PSRs host sub-regions that appear to be younger than the overall PSR. There appears to be no spatial trend in the distribution of younger and older PSRs, both are scattered across the study area.

3.4. PSR Temperature Regime

The studied PSRs feature a large range of temperatures. Four PSRs appear to remain at temperatures below ~110 K, the sublimation temperature of water ice (Schorghofer & Williams, 2020; Williams et al., 2019; Zhang & Paige, 2009), over the lunar year and might be particularly likely to trap volatiles over geologic and human timescales. All studied PSRs host temperatures below ~110 K at least once over the lunar year. All PSRs feature generally higher temperatures during the southern summer (ecliptic longitude ~270°) than during the southern

winter (ecliptic longitude ∼90°). However, the distribution of peak temperature as a function of the local time is highly heterogeneous—∼10 PSRs feature peak temperatures before noon, ∼12 around noon, ∼13 in the afternoon, ∼7 during the night, and ∼2 feature a bimodal temperature peak distribution. The influence of secondary illumination on the temperature regime in the studied PSRs is complex. There seems to be a distinct correlation between illumination geometry, local time, temperature, and the HORUS signal in many of the studied PSRs (pages S12–S278), which is highly unique to each PSR due to the important role of the local topography in scattering the primary illumination. We note that many of the studied PSRs might host super-cold doubly shadowed regions that are shielded from primary and secondary illumination (O'Brien & Byrne, 2022), for example, within umbral impact craters and underneath large, umbral boulders. Doubly-shadowed regions might host compounds that are more volatile than water ice, such as CO_2 (Landis et al., 2022; Schorghofer et al., 2021).

3.5. PSR Trafficability

Our mapping campaign did not produce any evidence that the studied PSRs in the Artemis exploration zone would not be trafficable, assuming that robotic assets and crew can navigate PSR entry slope angles of around ∼14°. Here, the entry slope angle is the inclination of a (close-to) rover-scale PSR terminator segment of a given PSR, thus, describing what slope angle must be overcome to cross the terminator of a given PSR. As far as resolved by HORUS, craters and boulders (with minimum diameters of around ∼3–4 m) do not present significant hazards and/or obstacles in any of the studied PSRs, although we stress that not all PSRs could be resolved down to ∼3–4 m due to a lack of secondary illumination. It remains unclear whether the smooth and textured surface features that were observed in some of the PSRs/TSRs feature anomalous geomechanical properties and whether they represent any potential hazard to future ground-based exploration efforts. We note that there are PSRs of all relative ages that appear to be particularly benign to exploration, featuring entry slope angles as low as ∼1°. We did not find direct evidence for a distal origin of the mapped umbral boulders, but note that the sub-surface bearing capacity (>∼0.75 m depth) of boulder-bearing PSRs (boulders >∼3 m) might be reasonably high, assuming that boulders have a distal origin, for example, through mass wasting (Bickel et al., 2021). As boulders smaller than ∼3 m are not resolved by HORUS, there are no implications for depths between the surface and ∼0.75 m, as for example, estimated by Sargeant et al. (2020) for a number of low latitude PSRs (with substantially better secondary illumination). We stress that our analysis does not provide any information about the geomechanical properties of the shallow sub-surface and surface of the studied PSRs—geomechanical anomalies are likely to occur, in shadowed and sunlit regions—and that our initial observations require in situ verification.

4. Exploration Recommendations

Our analysis shows that the 44 studied PSRs feature a wide range of geologic/geomorphic and thermophysical properties and characteristics. The attractiveness of a given PSR strongly depends on the scope and goals of a mission, as well as on the mobility capabilities of an asset and/or crew. For example, only ∼16 of the studied PSRs (∼36%) could be reached assuming a maximum one-way traverse length of 2 km (i.e., 4 km back and forth) as currently envisioned for the Artemis walking EVAs and assuming a lander would touch down anywhere on the well-lit Shackleton-Henson connecting ridge or Shackleton crater's rim. When considering this specific distance constraint, the following PSRs feature characteristics potentially attractive to future exploration:

1. **O01b**—is an intermediately old, particularly cold PSR which might feature surface ice according to M^3, modeled subsurface ice at a depth of ∼0.23 m, and a wide variety of boulders, lobate features, textured ground, and craters, including potentially fresher craters (Figure 3). However, access to its center might require a rover/astronaut to navigate slopes of up to ∼20°. In addition, there is zero Earth visibility (page S105).
2. **U01a**—is a younger and particularly small PSR on Shackleton crater's rim, very close to potential Artemis landing site 004, which features multiple boulders/outcrops and impact craters. This PSR might be the only permanently shadowed (younger) rocky crater with a diameter >∼100 m in the region, making it a unique target (Figure S2 in Supporting Information S1). However, access to its center might require a rover/astronaut to navigate steep slopes of up to ∼30° as well as potential accumulations of (undetected) umbral boulders <∼3 m in diameter (page S123).
3. **X01a**—is a small, intermediately, old and relatively warm PSR right next to site 001 that might potentially be targeted by IM-2's S. P. Hopper (Martin et al., 2022). We note that X01a hosts a ∼50 m-diameter crater and a number of other features, which might require S. P. Hopper to touch down in two specific sections of the PSR

to avoid potentially hazardous slopes and boulders (Figure 2, Figures S9 and S10, page S267 in Supporting Information S1).

4. **M01g,h & U01b,c,d & V01j**—are intermediately old to older, small PSRs on Shackleton crater's rim and/or the connecting ridge. They appear to be relatively warm with modeled ice stability depths of about >∼1 m (see, e.g., page S69), but appear to host potentially fresher craters and might be very accessible, with slope angles <∼15° and very few visible boulders and craters. PSR V01j appears to be particularly accessible with maximum slopes <∼10° (e.g., page S69). We note that some of those PSRs are poorly secondary-lit (specifically V01j), that is, might not be well characterized by HORUS.

Neglecting any limitation regarding traverse length, landing site location, and mobility, the following PSRs feature characteristics potentially attractive to future exploration:

5. **K01a,b & L01a**—are large and particularly cold PSRs that might feature (modeled) ice/frost on their surfaces (no M^3 detections), hosting a large variety of boulders, textured ground, and craters, including potentially fresher craters (Figure 3). Access to those PSRs appears to be relatively easy, with slope angles <∼5–∼10°, although they are not in the direct vicinity of either Shackleton crater rim or the connecting ridge. Both PSRs appear to feature younger and older sections, potentially providing comparative sampling opportunities to test models of volatile accumulation (pages S15, S21, and S27).
6. **O01a**—is a very large, particularly cold PSR. This is the only PSR in the study area that features both M^3 surface detections and modeled surface ice; that is, features the highest likelihood for surface-exposed volatiles (Figure 3). Remarkably, the temperature regime of this PSR seems to be stable over the seasons. This PSR hosts a large variety of craters, including potentially very fresh craters, but no boulders. Access to the PSR appears to be potentially challenging from the connecting ridge and Shackleton rim, but relatively easy from the West (slope angles <∼10°). O01a appears to have relatively younger and older sections, potentially providing comparative sampling opportunities (page S99).
7. **V01c**—is a small, intermediately old, relatively warm PSR with relatively steep slopes (max slope ∼25°) and a modeled ice stability depth of >∼2.5 m. In addition, there is zero Earth visibility. However, this PSR might potentially host one or even two very fresh impact craters that might be surrounded by bright ejecta of potentially excavated ice-rich blocks (Figure S4, page S183 in Supporting Information S1).
8. **W01e**—is a small, relatively warm PSR with modeled ice stability depth >2.5 m, distal to the connecting ridge and Shackleton crater rim. In addition, this PSR appears to be challenging to traverse (max slope angles of ∼29°), but features a unique geomorphology: potentially very fresh craters (could be rocky craters, Figure S3 in Supporting Information S1), prominently textured ground, as well as a very distinct contact between textured and smooth ground, only partially following the local contour lines (Figures S5–S7, page S255 in Supporting Information S1).

5. Conclusions

We used a deep learning-driven post-processing tool called HORUS to produce the first high-resolution, high-SNR NAC images of selected PSRs with diameters >∼40 m ($n = 44$) in a section of the Artemis exploration zone, close to the potential Artemis 001 and 004, IM-2, as well as other landing sites. We used those images to systematically map umbral craters, boulders, lobate features, and textured ground, down to a scale of ∼4 m. We did not observe any direct evidence of surface-exposed ice and/or frost, even in sites with M^3 detections and/or modeled ice surface stability, providing additional evidence that volatiles may be intermixed with the regolith or buried at depth. The PSR that will potentially be targeted by IM-2 appears to host a ∼50 m diameter crater as well as other features which might require S. P. Hopper to touch down within two specific, apparently smooth sections of the PSR. We discovered a number of potentially fresh impact craters across the studied PSRs—some with potential, faint indications of ejecta blankets—that might have excavated subsurface volatiles or facilitate access to them. We combined our HORUS-derived observations with existing geological and thermophysical products and compiled a detailed Artemis exploration zone PSR catalog, highlighting particularly promising PSR candidates for future exploration. The catalog and produced data products are freely available here: https://doi.org/10.56272/GQKZ6227. Our findings, detailed catalog (in the supplementary information), and data will have direct implications for all future exploration efforts in the Artemis exploration zone and the lunar polar regions in general.

Data Availability Statement

The raw LRO NAC image data used for this study is freely available on the PDS, for example, here: https://wms.lroc.asu.edu/lroc/search. Many of the auxiliary datasets used for the analysis, such as the LOLA DEM/slope (Barker et al., 2021), surface roughness (Smith & the LOLA Team, 2022), Earth visibility, and PSR maps (Mazarico et al., 2011) are freely available here: https://pgda.gsfc.nasa.gov/products/78, http://imbrium.mit.edu/, http://imbrium.mit.edu/EXTRAS/ILLUMINATION/, and http://imbrium.mit.edu/EXTRAS/FRACTAL/. All produced and validated HORUS images (8,888 images with a total size of ~4.5 TB, details in the supplementary information) can be accessed and retrieved via FDL's SpaceML website: https://doi.org/10.56272/GQKZ6227.

Acknowledgments
VTB thanks Jennifer Heldmann, Ariel Deutsch, Ross Beyer, Richard Elphic, Anthony Colaprete, and Matthew Atwell for fruitful discussions and valuable feedback. This work has been enabled by the Frontier Development Lab (FDL) which is a co-operative agreement between NASA (http://www.frontierdevelopmentlab.org/) and the SETI Institute (https://www.seti.org), and supported by the Luxembourg Space Agency, Google Cloud, and NVIDIA. VTB thanks Hannes Bernhardt for sharing the new 1:8000 Artemis 001 and 004 geomorphic map prior to its publication. JPW was supported by the Korea Pathfinder Lunar Orbiter (KPLO) Participating Scientist Program (PSP) under award number 80NSSC21K0711. DAK was supported by the NASA Solar System Exploration Research Virtual Institute through a cooperative agreement (80NSSC20M0016) for the LPI-JSC Center for Lunar Science and Exploration. LPI Contribution No. 2709. LPI is operated by USRA under a cooperative agreement with the Science Mission Directorate of the National Aeronautics and Space Administration.

References

Arnold, J. R. (1979). Ice in the lunar polar regions. *Journal of Geophysical Research*, *84*(B10), 5659–5668. https://doi.org/10.1029/JB084iB10p05659

Arvidson, R., Crozaz, G., Drozd, R. J., Hohenberg, C. M., & Morgan, C. J. (1975). Cosmic ray exposure ages of features and events at the Apollo landing sites. *The Moon*, *13*(1–3), 259–276. https://doi.org/10.1007/bf00567518

Barker, M. K., Mazarico, E., Neumann, G. A., Smith, D. E., Zuber, M. T., & Head, J. W. (2021). Improved LOLA elevation maps for south pole landing sites: Error estimates and their impact on illumination conditions. *Planetary and Space Science*, *203*, 105119. https://doi.org/10.1016/j.pss.2020.105119

Bernhardt, H., Robinson, M., & Boyd, A. (2022). Geomorphic map and science target identification on the Shackleton-de Gerlache ridge. *Icarus*, *379*, 114963. https://doi.org/10.1016/j.icarus.2022.114963

Bickel, V. T., & Kring, D. A. (2020). Lunar south pole boulders and boulder tracks: Implications for crew and rover traverses. *Icarus*, *348*, 113850. https://doi.org/10.1016/j.icarus.2020.113850

Bickel, V. T., Moseley, B., Lopez-Franco, I., & Shirley, M. (2021). Peering into lunar permanently shadowed regions with deep learning. *Nature Communications*, *12*(1), 5607. https://doi.org/10.1038/s41467-021-25882-z

Bogard, D. D., & Hirsch, W. C. (1978). Depositional and irradiational history and noble gas contents of orange-black droplets in the 74002/1 core from Shorty crater. In *Proceedings of the Lunar and Planetary Science Conference*, (Vol. *9*, pp. 1981–2000).

Cannon, K., Deutsch, A., Head, J., & Britt, D. (2020). Stratigraphy of ice and ejecta deposits at the lunar Poles. *Geophysical Research Letters*, *47*(21), e2020GL088920. https://doi.org/10.1029/2020GL088920

Cisneros, E., Awumah, A., Brown, A. C., Paris, K. N., Povilaitis, R. Z., Boyd, A. K., et al. (2017). Lunar reconnaissance orbiter camera permanently shadowed region imaging—Atlas and controlled Mosaics. In *48th lunar and planetary science conference* (p. 2469). Retrieved from https://www.hou.usra.edu/meetings/lpsc2017/eposter/2469.pdf

Colaprete, A., Elphic, R., Shirley, M., Ennico-Smith, K., Lim, D. S. S., Zacny, K., & Captain, J. (2021). The volatiles investigating polar exploration rover (VIPER) mission—Measurements and constraints. In *52nd lunar and planetary science conference* (p. 2898). Retrieved from https://www.hou.usra.edu/meetings/lpsc2021/pdf/1523.pdf

Deutsch, A. N., Head, J. W., Neumann, G. A., Kreslavsky, M. A., & Barker, M. K. (2020). Assessing the roughness properties of circumpolar lunar craters: Implications for the timing of water-ice delivery to the Moon. *Geophysical Research Letters*, *47*(15), e2020GL087782. https://doi.org/10.1029/2020GL087782

Drozd, R. K., Hohenberg, C. M., Morgan, C. J., & Ralston, C. E. (1974). Cosmic-ray exposure history at the Apollo 16 and other lunar sites: Lunar surface dynamics. *Geochimica et Cosmochimica Acta*, *38*(10), 1625–1642. https://doi.org/10.1016/0016-7037(74)90178-1

Ehlmann, B. L., Klima, R., Seybold, C. C., Klesh, A. T., Au, M. H., Bender, C. L., et al. (2022). *NASA's lunar trailblazer mission: A pioneering small satellite for lunar water and lunar geology* (pp. 1–14). IEEE Aerospace Conference. Retrieved from https://trailblazer.caltech.edu/files/Ehlmann_et al._2022_LunarTrailblazerMission_IEEEAero.pdf

Feldman, W. C., Maurice, S., Lawrence, D. J., Little, R. C., Lawson, S. L., Gasnault, O., et al. (2011). Evidence for water ice near the lunar poles. *Journal of Geophysical Research*, *106*(E10), 23231–23251. https://doi.org/10.1029/2000JE001444

Gawronska, A., Barrett, N., Boazman, S., Gilmoure, C., Halim, H., Harish, K., et al. (2020). Geologic context and potential EVA targets at the lunar south pole. *Advances in Space Research*, *66*(6), 1247–1264. https://doi.org/10.1016/j.asr.2020.05.035

Haruyama, J., Ohtake, M., Matsunaga, T., Morota, T., Honda, C., Yokota, Y., et al. (2008). Lack of exposed ice inside lunar south pole Shackleton crater. *Science*, *322*(5903), 938–939. https://doi.org/10.1126/science.1164020

Haruyama, J., Yamamoto, S., Yokota, Y., Ohtake, M., & Matsunaga, T. (2013). An explanation of bright areas inside Shackleton Crater at the lunar south pole other than water-ice deposits. *Geophysical Research Letters*, *40*(15), 3814–3818. https://doi.org/10.1002/grl.50753

Hayne, P., Aharonson, O., & Schörghofer, N. (2020). Micro cold traps on the Moon. *Nature Astronomy*, *5*(2), 169–175. https://doi.org/10.1038/s41550-020-1198-9

Kereszturi, A., Tomka, R., & Steinmann, V. (2022). Testing statistical impact crater analysis in permanently shadowed lunar polar regions. *Icarus*, *376*, 114879. https://doi.org/10.1016/j.icarus.2022.114879

Landis, M. E., Hayne, P. O., Williams, J.-P., Greenhagen, B. T., & Paige, D. A. (2022). Spatial distribution and thermal diversity of surface volatile cold traps at the lunar poles. *The Planetary Science Journal*, *3*(2), 39. https://doi.org/10.3847/PSJ/ac4585

Li, S., Lucey, P., Milliken, R., Elphic, R., Fisher, E., Williams, J. P., et al. (2018). Direct evidence of surface exposed water ice in the lunar polar regions. *Proceedings of the National Academy of Sciences of the United States of America*, *115*(36), 8907–8912. https://doi.org/10.1073/pnas.1802345115

Martin, A. C., Atwell, M., Oelke, M. L., Crain, T. P., Robinson, M. S., Wagner, R., et al. (2022). S. P. Hopper: First in-situ exploration of lunar polar terrain. In *53rd lunar and planetary science conference* (p. 2007). Retrieved from https://www.hou.usra.edu/meetings/lpsc2022/pdf/2007.pdf

Martin, A. C., Denevi, B. W., Speyerer, E., Thompson, J., Brown, H. M., Boyd, A. K., & Robinson, M. S. (2021). Comparison of images with direct and indirect illumination: Lunar permanently shadowed region analog images. In *52nd lunar and planetary science conference* (p. 2349). Retrieved from https://www.hou.usra.edu/meetings/lpsc2021/pdf/2349.pdf

Mazarico, E., Neumann, G. A., Smith, D. E., Zuber, M. T., & Torrence, M. H. (2011). Illumination conditions of the lunar polar regions using LOLA topography. *Icarus*, *211*(2), 1066–1081. https://doi.org/10.1016/j.icarus.2010.10.030

Moon, S., Paige, D., Siegler, M., & Russell, P. (2020). Geomorphic evidence for the presence of ice deposits in the permanently shadowed regions of Scott-E Crater on the Moon. *Geophysical Research Letters*, *48*(2), e2020GL090780. https://doi.org/10.1029/2020GL090780

Moseley, B., Bickel, V. T., Lopez-Francos, I., & Rana, L. (2021). Extreme low-light environment-driven image denoising over permanently shadowed lunar regions with a physical noise model. In *Proceedings of the IEEE/CVF conference on computer vision and pattern recognition (CVPR)*.

NASA. (2020a). Artemis III science definition team report. Report No. NASA/SP-20205009602.

NASA. (2020b). NASA's plan for sustained lunar exploration and development.

Needham, D. H., & Kring, D. A. (2017). *Lunar volcanism produced a transient atmosphere around the ancient Moon* (Vol. 478, pp. 175–178). Earth and Planetary Science Letters. Retrieved from https://ui.adsabs.harvard.edu/abs/2017E%26PSL.478..175N/abstract

O'Brien, P., & Byrne, S. (2022). Cooler than cool: Doubly shadowed regions at the lunar Poles. In *53rd lunar and planetary science conference 2022*. Retrieved from https://www.hou.usra.edu/meetings/lpsc2022/pdf/2372.pdf

Paige, D. A., Siegler, M. A., Zhang, J. A., Hayne, P. O., Foote, E. J., Bennett, K. A., et al. (2010). Diviner lunar radiometer observations of cold traps in the Moon's south polar region. *Science*, *330*(6003), 479–482. https://doi.org/10.1126/science.1187726

Sargeant, H. M., Bickel, V. T., Honniball, C., Martinez, S., Rogaski, A., Bell, S., et al. (2020). Using boulder tracks as a tool to understand the bearing capacity of permanently shadowed regions of the Moon. *Journal of Geophysical Research: Planets*, *125*(2), e2019JE006157. https://doi.org/10.1029/2019JE006157

Schorghofer, N., & Williams, J.-P. (2020). Mapping of ice storage processes on the Moon with time-dependent temperatures. *The Planetary Science Journal*, *1*(3), 54. https://doi.org/10.3847/PSJ/abb6ff

Schorghofer, N., Williams, J.-P., Martinez-Camacho, J., Paige, D. A., & Siegler, M. A. (2021). Carbon dioxide cold traps on the Moon. *Geophysical Research Letters*, *48*(20), e2021GL095533. https://doi.org/10.1029/2021GL095533

Scoville, Z. C. (2022). Artemis III EVA mission capability for de Gerlache-Shackleton ridge. In *53rd lunar and planetary science conference 2022*. Retrieved from https://www.hou.usra.edu/meetings/lpsc2022/pdf/1079.pdf

ShadowCam. (2022). Seeing in the shadows – science objectives. Retrieved from http://shadowcam.sese.asu.edu/about

Siegler, M., Miller, R., Keane, J., Laneuville, M., Paige, D., Matsuyama, I., et al. (2016). Lunar true polar wander inferred from polar hydrogen. *Nature*, *531*(7595), 480–484. https://doi.org/10.1038/nature17166

Smith, D. E., & the LOLA Team. (2022). LRO-L-LOLA-4-GDR-V1.0 LDRM_85S_40M. Retrieved from https://pds-geosciences.wustl.edu/lro/lro-l-lola-3-rdr-v1/lrolol_1xxx/data/lola_gdr/polar/img/ldrm_85s_40m.lbl

Speyerer, E., & Robinson, M. (2013). Persistently illuminated regions at the lunar poles: Ideal sites for future exploration. *Icarus*, *222*(1), 122–136. https://doi.org/10.1016/j.icarus.2012.10.010

Spudis, P., Bussey, B., Plescia, J., Josset, J.-L., & Beauvivre, S. (2008). Geology of Shackleton crater and the south pole of the Moon. *Geophysical Research Letters*, *34*(14), L14201. https://doi.org/10.1029/2008GL034468

Watson, K., Murray, B., & Brown, H. (1961). On the possible presence of ice on the Moon. *Journal of Geophysical Research*, *66*(5), 1598–1600. https://doi.org/10.1029/JZ066i005p01598

Williams, J.-P., Greenhagen, B., Paige, D., Schorghofer, N., Sefton-Nash, E., Hayne, P., et al. (2019). Seasonal polar temperatures on the Moon. *Journal of Geophysical Research: Planets*, *124*(10), 2505–2521. https://doi.org/10.1029/2019JE006028

Zhang, J. A., & Paige, D. A. (2009). Cold-trapped organic compounds at the poles of the Moon and Mercury: Implications for origins. *Geophysical Research Letters*, *36*(16), L16203. https://doi.org/10.1029/2009GL038614

References From the Supporting Information

Deutsch, A., Heldmann, J., Colaprete, A., Cannon, K., & Elphic, R. (2021). Analyzing surface ruggedness inside and outside of ice stability zones at the lunar Poles. *The Planetary Science Journal*, *2*(5), 213. https://doi.org/10.3847/PSJ/ac24ff

LMMP. (2011). LRO LROC NAC image mosaic, S Pole, avg merge. Retrieved from https://trek.nasa.gov/moon/TrekWS/rest/cat/metadata/fgdc/html?label=LRO_NAC_AvgMosaic_SPole855_1mp

Riedel, C., Michael, G. G., Kneissl, T., Orgel, C., Hiesinger, H., & van der Bogert, C. H. (2018). A new tool to account for crater obliteration effects in crater size-frequency distribution measurements. *Earth and Space Science*, *5*(6), 258–267. https://doi.org/10.1002/2018EA000383